JOURNAL OF SPACECRAFT AND ROCKETS
Vol. 34, No. 3, May–June 1997

Dynamic Model for Global Positioning System Block IIR Space Vehicle

C. S. Lin* and T. R. Cole†
The Aerospace Corporation, El Segundo, California 90245

The authors describe the development of the dynamic model for the Global Positioning System Block IIR space vehicle. A mode survey test was conducted for each of the spacecraft and the solar array assemblies to obtain a test-derived dynamic model. In the spacecraft mode survey, the attachment clampband was found not rigid enough to produce fixed-base normal modes. An analytical technique was developed to remove the effects of the clampband flexibility from the measured spacecraft modes. The test-derived spacecraft and solar array assembly models were coupled using the component modal synthesis method to form the system dynamic model to be used in the coupled-system loads analysis. The spacecraft finite element model was adjusted to correlate with the mode test data to improve the accuracy of the loads transformation matrix.

Nomenclature

f	= flexibility matrix
I	= identity matrix
K	= stiffness matrix
K_b	= clampband stiffness matrix
$\hat{K}$	= generalized stiffness matrix in modal coordinates
M	= mass matrix
M_{er}	= modal effective mass
$\bar{M}$	= generalized mass matrix in relative coordinates
$\hat{M}$	= generalized mass matrix in modal coordinates
q, q', q''	= generalized modal coordinates
T	= rigid-body transformation matrix due to unit displacements at interface
x	= displacement for test configuration
$\ddot{x}$	= acceleration for test configuration
x'	= displacement for fixed-interface configuration
$\ddot{x}'$	= acceleration for fixed-interface configuration
ΔK	= differential stiffness matrix due to changes in boundary conditions
ΔM	= differential mass matrix due to changes in boundary conditions
ϕ	= modal matrix
ϕ'	= modal matrix for fixed-interface configuration
ψ	= fixed-interface modal matrix in generalized coordinates
ω	= circular natural frequency
ω'	= fixed-interface circular natural frequency
$\odot$	= element-by-element multiplication

Subscripts

i	= interface degree of freedom
n	= noninterface degree of freedom
nr	= noninterface displacement or mode shape relative to interface

Introduction

THE Block IIR satellites of the Global Positioning System (GPS) (Fig. 1) are to be launched to replenish the GPS system of 24 satellites. To ensure accurate prediction of dynamic loads occurring during launch and ascent, the spacecraft contractor was required to conduct a mode survey test on the satellite structure to measure its dynamic characteristics. Because of the complexity of the satellite structure, modification of the finite element model to produce normal modes and frequencies in agreement with the mode survey results was expected to be difficult and unlikely to yield a satisfactory dynamic model within the program time constraint. Therefore, the program loads analysis plan specified the use of measured normal modes and frequencies to represent the satellite in the form of a generalized dynamic model in the integrated launch-vehicle–satellite system loads analysis, a common practice for the U.S. Air Force space programs.[1] Nevertheless, since the finite element model was used in developing the loads transformation matrix, the loads analysis plan also specified that the finite element model be adjusted based on the mode survey data.

The mode survey of the Block IIR satellite was conducted during 1994 in two parts, namely, the supported stowed solar array survey and the cantilevered spacecraft survey. The latter test used mass simulators for the stowed solar arrays. The overall satellite dynamic model was formulated by combining the test-derived data obtained from these two surveys using the component modal synthesis method.[2,3] Only the spacecraft survey will be considered of interest in this paper because of a peculiar boundary-condition problem associated with its use of a clampband assembly connecting the spacecraft to the rigid test fixture. The clampband assembly comprises mating rings, shoes, and straps. The two rings, attached to the spacecraft and the test fixture (or the upper stage for the flight configuration), respectively, are clamped together by the shoes, which are preloaded radially by tensile forces in the straps. The force–displacement relations for such an assembly are nonlinear. For the dynamic loads analysis, however, a set of equivalent linear stiffness coefficients are typically determined by tests to form a linear model.

For the GPS IIR spacecraft mode survey, the clampband was expected to be sufficiently rigid to produce fixed-base normal modes. However, it was found in the preliminary posttest assessment that the clampband was not as rigid as expected. The clampband created a local flexibility at the base intermediate to a flight configuration and a fixed configuration. The launch vehicle contractor required a fixed-interface spacecraft model for the integrated system loads analysis. The interface clampband flexibility was already included in the upper-stage dynamic model. The overall upper-stage dynamic model had been verified by another mode survey test,[4] which included the clampband and a rigid spacecraft simulator with representative local flexibility in the vicinity of the clampband interface.

To address the clampband flexibility concern, the authors developed an analytical technique to remove the effects of the clampband flexibility from the measured modes. In addition to presenting this analytical technique, this paper describes a systematic trial-and-error approach taken to correlate the spacecraft finite element

Received June 26, 1996; revision received Feb. 24, 1997; accepted for publication Feb. 25, 1997.

*Engineering Specialist, Structural Dynamics Department. Senior Member AIAA.

†Senior Member, Technical Staff, Structural Dynamics Department. Member AIAA.

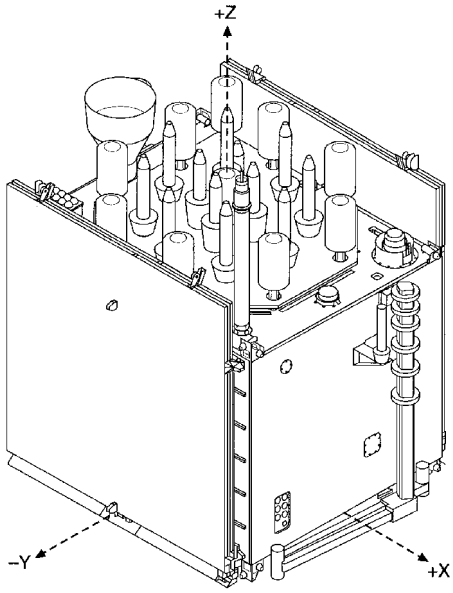

Fig. 1 GPS IIR space vehicle in stowed configuration.

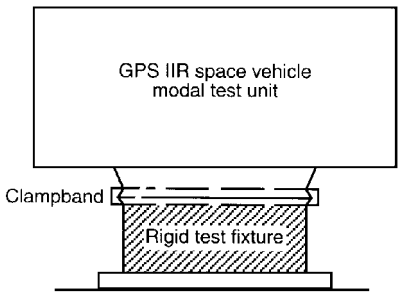

Fig. 2 Schematic of spacecraft mode survey test article.

model with the mode test data. These elaborate efforts result in not only a reliable test-derived model for dynamic loads analysis but also a test-correlated finite element model for calculating the loads transformation matrix.

Space Vehicle Mode Survey Test

The space vehicle mode survey test was conducted during August through October 1994 at the Valley Forge Dynamic Simulation Laboratory of Lockheed Martin Astro Space.[5] The test article comprised the flight core structure with mass simulators for the solar arrays, fuel tanks, the apogee kick motor, and most sensors and components. The test article, which weighed 2047 kg, was attached at the base of the flight adapter ring to a rigid test fixture by the flight clampband as shown in Fig. 2. A total of 244 piezoelectric accelerometers were used to map the mode shapes. Frequency response functions obtained from the test were processed to estimate the mode shapes, frequencies, and damping values. A total of 13 modes were identified within the frequency range of interest, 0–50 Hz (Table 1). The orthogonality matrix of the measured modes (Table 2) was judged satisfactory.

Modification of Measured Modes

Since the clampband interface was found to be too flexible to produce fixed-base modes, the following procedure was developed to modify the measured modes. First, since the clampband interface plane was relatively rigid, it was assumed to remain plane during the test. Therefore, the interface motion was represented by a single node with six degrees of freedom (DOFs), and the clampband stiffness by a set of six corresponding stiffness constants. The equations of free vibration for the spacecraft during the mode survey test (Fig. 3) can be represented by

$$\begin{bmatrix} M_{nn} & M_{ni} \\ M_{in} & M_{ii} \end{bmatrix} \begin{Bmatrix} \ddot{x}_n \\ \ddot{x}_i \end{Bmatrix} + \begin{bmatrix} K_{nn} & K_{ni} \\ K_{in} & K_{ii} + K_b \end{bmatrix} \begin{Bmatrix} x_n \\ x_i \end{Bmatrix} = \begin{Bmatrix} 0 \\ 0 \end{Bmatrix} \tag{1}$$

Table 1 GPS IIR SV measured modes

Mode no.	Frequency, Hz	Mode description
1	21.27	$-X$ payload panel
2	24.26	Vehicle X-dir. bending
3	26.05	Vehicle Y-dir. bending
4	27.86	S-band antenna, X dir.
5	33.33	S-band antenna, Y dir.
6	35.75	Vehicle torsion
7	38.63	$+X$ bus panel
8	39.30	$-X$ bus panel
9	40.28	Mission data unit; $-X$ payload panel
10	45.35	$-X$ bulkhead
11	47.29	Vehicle axial
12	48.31	Burst detector dosimeter
13	49.31	$+X$ payload panel

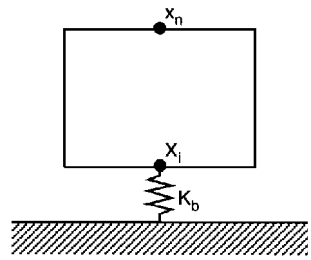

Fig. 3 Spacecraft with flexible-base boundary.

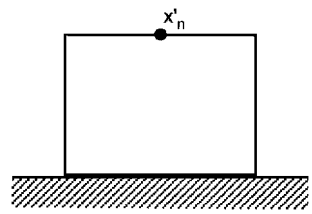

Fig. 4 Spacecraft with fixed-base boundary.

Similarly, the equation for the spacecraft in the desired fixed-interface configuration (Fig. 4) can be expressed as

$$[M_{nn}]\{\ddot{x}'_n\} + [K_{nn}]\{x'_n\} = \{0\} \tag{2}$$

To estimate the modes and frequencies for Eq. (2), one can approximate its mode shapes by those of Eq. (1). Since the mode shapes for Eq. (2) involve no base motion, the approximation can be more accurately achieved by expressing the Eq. (1) mode shapes in coordinates relative to the interface DOFs instead of absolute coordinates. Toward that end, Eq. (1) will be transformed into the relative coordinates. The noninterface displacements relative to the interface can be defined as

$$\{x_{nr}\} = \{x_n\} - [T]\{x_i\} \tag{3}$$

Then it follows that

$$\begin{Bmatrix} x_n \\ x_i \end{Bmatrix} = \begin{bmatrix} I & T \\ 0 & I \end{bmatrix} \begin{Bmatrix} x_{nr} \\ x_i \end{Bmatrix} \tag{4}$$

Since an unconstrained spacecraft undergoes rigid-body motion without producing any internal forces, the following is also true:

$$\begin{bmatrix} K_{nn} & K_{ni} \\ K_{in} & K_{ii} \end{bmatrix} \begin{bmatrix} T \\ I \end{bmatrix} = \begin{bmatrix} 0 \\ 0 \end{bmatrix} \tag{5}$$

Using Eqs. (4) and (5), Eq. (1) can be transformed into the relative coordinates as follows:

$$\begin{bmatrix} M_{nn} & \bar{M}_{ni} \\ \bar{M}_{in} & \bar{M}_{ii} \end{bmatrix} \begin{Bmatrix} \ddot{x}_{nr} \\ \ddot{x}_i \end{Bmatrix} + \begin{bmatrix} K_{nn} & 0 \\ 0 & K_b \end{bmatrix} \begin{Bmatrix} x_{nr} \\ x_i \end{Bmatrix} = \begin{Bmatrix} 0 \\ 0 \end{Bmatrix} \tag{6}$$

where

$$[\bar{M}_{ni}] = [\bar{M}_{in}]^T = [M_{ni}] + [M_{nn}][T]$$

$$[\bar{M}_{ii}] = [M_{ii}] + [M_{in}][T] + [T]^T[M_{ni}] + [T]^T[M_{nn}][T]$$

The measured modes are similarly transformed into the relative coordinates as follows:

$$\begin{bmatrix}\phi_{nr}\\ \phi_i\end{bmatrix} = \begin{bmatrix}I & -T\\ 0 & I\end{bmatrix}\begin{bmatrix}\phi_n\\ \phi_i\end{bmatrix} \tag{7}$$

Since the interface clampband was expected to be sufficiently rigid in the mode test, insufficient measurements were made at the interface to define ϕ_i. Therefore, it was decided to obtain the interface mode shape values from the noninterface mode shape values by the transformation developed from the static condensation of the stiffness matrix,[6] namely,

$$[\phi_i] = -[K_{ii} + K_b]^{-1}[K_{in}][\phi_n] \tag{8}$$

The expanded modes are then orthogonalized using the Targoff method.[7] Furthermore, letting

$$\begin{Bmatrix}x_{nr}\\ x_i\end{Bmatrix} = \begin{bmatrix}\phi_{nr}\\ \phi_i\end{bmatrix}\{q\} \tag{9}$$

Equation (6) can be transformed into normal coordinates as follows:

$$[\hat{M}]\{\ddot{q}\} + [\hat{K}]\{q\} = \{0\} \tag{10}$$

where

$$[\hat{M}] = [\phi_{nr}]^T[M_{nn}][\phi_{nr}] + [\Delta M] = [I] \tag{11}$$

$$[\Delta M] = [\phi_i]^T[\bar{M}_{ii}][\phi_i] + [\phi_i]^T[\bar{M}_{in}][\phi_{nr}] + [\phi_{nr}]^T[\bar{M}_{ni}][\phi_i] \tag{12}$$

$$[\hat{K}] = [\phi_{nr}]^T[K_{nn}][\phi_{nr}] + [\Delta K] = [\omega^2] \tag{13}$$

$$[\Delta K] = [\phi_i]^T[K_b][\phi_i] \tag{14}$$

The natural frequency for the test configuration ω will be replaced by the measured frequency.

Let the spacecraft displacements in the fixed-interface configuration be represented by the relative mode shapes of Eq. (9), namely,

$$\{x_n'\} = [\phi_{nr}]\{q'\} \tag{15}$$

Then Eq. (2) becomes

$$[\phi_{nr}]^T[M_{nn}][\phi_{nr}]\{\ddot{q}'\} + [\phi_{nr}]^T[K_{nn}][\phi_{nr}]\{q'\} = \{0\} \tag{16}$$

Substituting Eqs. (11) and (13) into Eq. (16), the following is obtained:

$$[I - \Delta M]\{\ddot{q}'\} + [\omega^2 - \Delta K]\{q'\} = \{0\} \tag{17}$$

Equation (17) can be solved to obtain the fixed-interface normal modes (in generalized coordinates) and frequencies:

$$\{q'\} = [\psi]\{q''\} \tag{18}$$

Substituting Eq. (18) into Eq. (15), the mode shapes in physical coordinates can be obtained:

$$[\phi'] = [\phi_{nr}][\psi] \tag{19}$$

The resulting modes are orthogonal with respect to the analytical mass matrix.

For a given set of clampband stiffness values, the above procedure can be used to modify the measured modes to obtain approximate fixed-base modes. The procedure was first validated by applying it to a set of predicted flexible-base modes using the GPS IIR finite element model; the resulting set of modes agreed with the predicted fixed-base modes. Although a set of clampband stiffness values corresponding to the flight configuration was provided by the launch vehicle contractor, the actual test configuration stiffness values were different and not completely known. The test values were determined by an iterative trial-and-error process of correlating the finite element model and the test results, i.e., the clampband stiffness was treated as one of the parameters to be adjusted in the model correlation effort.

Model Correlation

Because of the complexity of the vehicle, the space-vehicle finite element model used approximately 54,000 DOFs to represent all important components and structural details. The model was then reduced by the Guyan method[8] to 244 dynamic DOFs corresponding to those measured in the test to define the mode shapes.

Preliminary adjustments were first made to correlate the model with the mode-test data. When the predicted fixed-base modes were compared with the measured modes, it was found that the predicted bending and axial frequencies were about 7–10% higher than the measured values (first column in Table 3). When the flight clampband stiffness values were incorporated into the analytical model, the predicted bending frequencies became lower than the measured values, while the predicted axial frequency remained higher than the measured value (second column in Table 3). Judging from the ranges of the frequency changes, the clampband flexibility appeared to have significant effects on the primary bending and axial modes. A sensitivity study was then performed to obtain a preliminary set of clampband stiffness values, which produced bending and axial mode frequencies that agree with the measured values (third column in Table 3). Using these clampband stiffness values, the frequencies predicted by the finite element model agreed reasonably well with

Table 3 Predicted frequency errors during preliminary adjustment of clampband stiffness[a]

SV primary mode description	1) Fixed-base configuration, %	2) Flight clampband stiffness, %	3) Preliminary clampband stiffness, %
Bending in X dir.	9.9	−26.3	0.6
Bending in Y dir.	8.0	−12.1	0.2
Torsional	−0.1	−0.7	−1.6
Axial	7.6	4.8	1.6

[a]A positive percentage error means the predicted frequency is higher than the measured frequency.

Table 2 Orthogonality check for GPS IIR spacecraft measured modes[a]

Mode	1	2	3	4	5	6	7	8	9	10	11	12	13
1	1.00												
2		1.00											
3			1.00										
4				1.00									
5					1.00	0.11							
6					0.11	1.00							
7							1.00						
8								1.00					
9									1.00				
10										1.00		0.11	
11											1.00	0.12	
12										0.11	0.12	1.00	
13													1.00

[a]Only entries >0.10 are shown.

Table 4 Comparison of measured frequencies vs predicted frequencies using preliminary adjusted model

Mode no.	Measured frequency, Hz	Predicted frequency, Hz	Difference, %
1	21.27	21.28	0.0
2	24.26	24.40	0.6
3	26.05	26.09	0.2
4	27.86	29.03	4.2
5	33.33	32.83	−1.5
6	35.75	35.18	−1.6
7	38.63	37.95	−1.8
8	39.30	39.48	0.5
9	40.28	40.32	0.1
10	45.35	45.55	0.4
11	47.29	48.03	1.6
12	48.31	48.69	0.8
13	49.31	49.79	1.0

Table 5 Comparison of final adjusted clampband stiffness values vs flight clampband stiffness values

Component[a]	Flight	Final	Factor
X	6.896E+09	4.203E+10	6.09
Y	6.896E+09	4.203E+10	6.09
Z	7.880E+08	1.051E+09	1.33
RX	5.629E+07	1.356E+9	24.09
RY	5.629E+07	1.356E+9	24.09
RZ	1.017E+09	1.412E+9	1.39

[a]Components of stiffness are expressed in GPS IIR coordinate system. Units for translational stiffness are N/m; units for rotational stiffness are N · m/rad.

Table 6 Comparison of measured frequencies vs predicted frequencies using final adjusted model

Mode no.	Measured frequency, Hz	Predicted frequency, Hz	Difference, %
1	21.27	21.20	−0.4
2	24.26	24.28	0.0
3	26.05	25.87	−0.7
4	27.86	29.00	4.1
5	33.33	32.77	−1.7
6	35.75	34.66	−3.0
7	38.63	37.35	−3.3
8	39.30	39.14	−0.4
9	40.28	39.95	−0.8
10	45.35	47.27	4.2
11	47.29	48.02	1.5
12	48.31	48.46	0.3
13	49.31	48.84	−1.0

the measured frequencies (Table 4). With the measured modes orthogonalized by the Targoff method, the cross-orthogonality check between the measured and predicted modes would have been considered satisfactory, except that the sixth and seventh modes had a 0.24 off-diagonal term. In the aerospace industry, typically, the goal is to keep all off-diagonal terms below 0.10.

It was found later that the flight clampband stiffness represented a set of equivalent stiffness values that included the flexibility of the clampband separation system and the adjacent local structures on both the space vehicle and the upper-stage sides. Since in the spacecraft mode test configuration the clampband was attached to a rigid test fixture on the upper-stage side, all of its stiffness values should be greater than those of the flight configuration. The preliminary clampband axial (Z) and torsional (RZ) stiffness values, which were significantly lower than those of the flight configuration, were found unreasonable.

The above observation was also corroborated by the comparisons of flexibility coefficients, modal effective mass, and modal kinetic energy distribution. The comparisons were made between those calculated from the measured and predicted modes. The flexibility coefficients were calculated as follows[9−11]:

$$[f] = [\phi][\omega^{-2}][\phi]^T$$

Only the diagonal terms were used to evaluate the flexibility at each DOF. The modal effective mass is defined as the element-by-element square of the modal participation matrix

$$[M_{er}] = [\phi]^T[M][T]$$

The modal kinetic energy was defined as follows:

$$[\phi] \odot ([M][\phi])$$

The calculated kinetic energy represents the contribution of each DOF to the generalized mass of unity for each mode. Through these comparisons, it was discovered that the clampband axial stiffnesss was too small and the longitudinal stiffness of the superstructure (structure above the clampband) was too large. It is likely that cancellation of these two effects resulted in the satisfactory frequency comparison and acceptable cross-orthogonality check, which are only indications of overall correlation and cannot ensure correct stiffness distribution in the model.

Additionally, the measured and predicted mode shapes were animated to facilitate locating modeling errors in the superstructure. Areas identified for potential correction included secondary structure support and attachment hardware and joint lines between primary structure items. These areas involved many types of joints, whose rigidity or stiffness was established in the original model mostly on the basis of experience and engineering judgment. By adjusting the joint and clampband stiffness values iteratively, a correlated model gradually emerged. The final set of the adjusted clampband stiffness values are shown in Table 5. The predicted frequencies using the final adjusted model agreed reasonable well with the measured frequencies (Table 6), and the cross-orthogonality (Table 7)

Table 7 Cross-orthogonality check: measured modes (columns) vs predicted modes using final adjusted model (rows)[a]

Frequency, Hz	Mode	21.27 1	24.26 2	26.05 3	27.86 4	33.33 5	35.75 6	38.63 7	39.30 8	40.28 9	45.35 10	47.29 11	48.31 12	49.31 13
21.20	1	0.99												
24.28	2		0.99											
25.87	3			−0.99										
29.00	4				1.00									
32.77	5					−0.99								
34.66	6						0.98							
37.35	7							0.97						
39.14	8								0.96					
39.95	9								0.11	−0.99				
47.27	10										−0.92			0.13
48.02	11											−0.95	−0.19	
48.46	12											0.17	−0.94	0.12
48.84	13										−0.11		−0.13	−0.94

[a]Only entries >0.10 are shown.

Table 8 Comparison of measured flexible-base frequencies and converted fixed-base frequencies

Mode description	Flexible-base mode, Hz	Fixed-base mode, Hz	Difference, %
$-X$ payload panel	21.27	21.38	0.5
Vehicle X-dir. bending	24.26	24.78	2.1
Vehicle Y-dir. bending	26.05	26.50	1.7
S-band antenna, X-dir.	27.86	27.88	0.1
S-band antenna, Y-dir.	33.33	33.34	0.0
Vehicle torsion	35.75	36.02	0.8
$+X$ bus panel	38.63	38.73	0.3
$-X$ bus panel	39.30	39.39	0.2
Mission data unit; $-X$ payload panel	40.28	40.41	0.3
$-X$ bulkhead	45.35	45.39	0.1
Vehicle axial	47.29	49.23	4.1
Burst detector dosimeter	48.31	48.30	0.0
$+X$ payload panel	49.31	49.35	0.1

Table 9 Comparison of fixed-base frequencies before and after updating

Mode description	Before, Hz	After, Hz	Change, %
$-X$ payload panel	21.38	21.38	0.0
Vehicle X-dir. bending	24.78	24.76	−0.1
Vehicle Y-dir. bending	26.50	26.40	−0.4
S-band antenna, X-dir.	27.88	27.88	0.0
S-band antenna, Y-dir.	33.34	33.34	0.0
Vehicle torsion	36.02	35.86	−0.4
$+X$ bus panel	38.73	38.56	−0.5
$-X$ bus panel	39.39	39.36	−0.1
Mission data unit; $-X$ payload panel	40.41	40.40	0.0
$-X$ bulkhead	45.39	45.44	0.1
Burst detector dosimeter	48.30	48.29	0.0
Vehicle axial	49.23	49.25	0.0
$+X$ payload panel	49.35	43.72	−11.4

showed some improvement over that of the preliminary adjusted model.

The final set of clampband stiffness values was used to convert the flexible-base measured modes into fixed-base modes. The frequency comparisons are shown in Table 8. The axial mode frequency was increased by 4.1%. The overall effects of the clampband flexibility turned out to be less significant than expected initially from the parametric study results shown in Table 3. The cross-orthogonality between the converted measured fixed-base modes and the final adjusted finite element fixed-base modes was as satisfactory as that of the flexible-base configuration (Table 7).

Model Updating and Coupling

After the mode survey test, the space vehicle underwent some local design changes. The effects of these changes on the normal modes and frequencies were taken into account analytically by adding the mass and stiffness changes to the fixed-base free-vibration equation of motion. The equation was transformed into the modal coordinates of the model, and then solved for the updated frequencies and mode shapes. A comparison of the frequencies before and after the updating is shown in Table 9. The updates produced changes only to one local mode, and the primary structure modes were not significantly affected. As a consistency check, the updating was alternatively performed first on the flexible-base modes, and the resulting modes were then converted into the fixed-base modes. Identical updated fixed-base modes were obtained.

The updated fixed-base spacecraft model was then coupled with the solar array models to form the flight configuration space vehicle model using the Benfield–Hruda approach.[12] The final space vehicle model was formed in the Hurty–Craig–Bampton format.[2,13] The coupling transformation matrices and the measured component critical damping ratios were used to form the coupled-system damping matrix, wherein the off-diagonal terms were not significant and were therefore ignored.

Discussion

The work on the GPS IIR model improvement indicated that a satisfactory cross-orthogonality check is a necessary condition, but not a sufficient condition, for a test-correlated model. The preliminary adjusted finite element model and the preliminary clampband stiffness values could have passed as a valid model for the test configuration if the judgement had been based only on the frequency comparisons and the cross-orthogonality check. Prompted by the finding of the unreasonableness of the preliminary clampband stiffness, a series of detailed comparisons of flexibility coefficients, modal kinetic energy distributions, and modal effective mass were performed. Some critical stiffness parameters in the finite element model were adjusted so that the predicted modes agreed reasonably well with the measured modes in both flexible- and fixed-base configurations. The resulting finite element model was used in developing the loads transformation matrix, and the clampband stiffness was used in converting the measured modes into fixed-base modes.

In general, the test-derived model is more desirable than the adjusted finite element model for the loads analysis because it can be achieved within a shorter and more predictable period of time. On the other hand, the adjusted finite element model can adapt more easily to changes and discrepancies, but it is more difficult to obtain and there is no guarantee that satisfactory correlation between test and analysis can be achieved within budget and schedule. For GPS IIR, although the program specified the use of the test-derived model, the adjusted finite element model should be equally acceptable for loads analysis because of the good correlation between predicted and measured modes.

Conclusion

It has been demonstrated that the proposed analytical technique to remove the effects of the flexible clampband is effective in mitigating boundary flexibility problems in mode surveys of large space vehicles. The application of the technique to the GPS IIR mode survey produced a satisfactory empirical fixed-base dynamic model to support the integrated system loads analysis. It has also been shown that to correlate a large, complex finite element model with mode test data is a difficult but possible task. Using various analytical tools to help locate the modeling errors, the elaborate trial-and-error approach did result in a satisfactory finite element model for the GPS IIR space vehicle.

Acknowledgments

This work was performed as a part of The Aerospace Corporation's general system engineering and integration support to the Global Positioning System Joint Program Office, under the auspices of K. Harendza. Lockheed Martin Astro Space (LMAS) is the spacecraft contractor, and McDonnell Douglas Aerospace is the launch vehicle contractor. The model correlation efforts were performed in cooperation with J. Peir, R. Agarwal, and J. Sturges of LMAS. Their contributions and courtesy are greatly appreciated. The authors would also like to thank W. Lee, R. Wagner, and H. Rakijian of The Aerospace Corporation for their encouragement and guidance.

References

[1]Fleming, E. R., "The Use of Component Mode Synthesis in the Dynamic Analysis of Aerospace Systems," *Combined Experimental/Analytical Modeling of Dynamic Structural Systems*, edited by D. R. Martinez and A. K. Miller, AMD Vol. 67, American Society of Mechanical Engineers, New York, 1985, pp. 155–165.

[2]Craig, R. R., *Structural Dynamics: An Introduction to Computer Methods*, 1st ed., Wiley, New York, 1981, pp. 467–495.

[3]Coppolino, R. N., "Hybrid Experimental/Analytical Dynamic Models of Aerospace Structures," *Combined Experimental/Analytical Modeling of Dynamic Structural Systems*, edited by D. R. Martinez and A. K. Miller, AMD Vol. 67, American Society of Mechanical Engineers, New York, 1985, pp. 79–107.

[4]Zorkocy, R. J., "PAM-DII 37" PAF Modal Survey Test," McDonnell Douglas Astronautics Co., Test Documentation Drawing 1T57610, Huntington Beach, CA, Jan. 1984.

[5]Howard, C., "GPS IIR Modal Survey Report," Lockheed Martin Astro Space, Rept. MA95-GPSIIR-002, Valley Forge, PA, Jan. 1995.

[6]Clough, R. W., and Penzien, J., *Dynamics of Structures*, 1st ed., McGraw–Hill, New York, 1975, pp. 172, 173.

[7]Targoff, W. P., "Orthogonality Check and Correction of Measured Modes," *AIAA Journal*, Vol. 14, No. 2, 1976, pp. 164–167.

[8]Guyan, R. J., "Reduction of Stiffness and Mass Matrices," *AIAA Journal*, Vol. 3, No. 2, 1965, p. 380.

[9]Berman, A., and Flannelly, W. G., "Theory of Incomplete Models of Dynamic Structures," *AIAA Journal*, Vol. 9, No. 8, 1971, pp. 1481–1487.

[10]Lin, C. S., "Location of Modeling Errors Using Modal Test Data," *AIAA Journal*, Vol. 28, No. 9, 1990, pp. 1650–1654.

[11]Lin, C. S., "Unity Check Method for Structural Damage Detection," *Proceedings of the AIAA Dynamics Specialists Conference* (Hilton Head, SC), AIAA, Washington, DC, 1994, pp. 347–354.

[12]Benfield, W. A., and Hruda, R. F., "Vibration Analysis of Structures by Component Mode Substitution," *AIAA Journal*, Vol. 9, No. 7, 1971, pp. 1255–1261.

[13]Hurty, W. C., "Dynamic Analysis of Structural Systems Using Component Modes," *AIAA Journal*, Vol. 3, No. 4, 1965, pp. 678–685.

R. B. Malla
Associate Editor